Review article **Open Access**

Nobuyuki Matsuda and Hiroki Takesue*

Generation and manipulation of entangled photons on silicon chips

DOI 10.1515/nanoph-2015-0148
Received November 28, 2015; revised January 23, 2016; accepted February 9, 2016

Abstract: Integrated quantum photonics is now seen as one of the promising approaches to realize scalable quantum information systems. With optical waveguides based on silicon photonics technologies, we can realize quantum optical circuits with a higher degree of integration than with silica waveguides. In addition, thanks to the large nonlinearity observed in silicon nanophotonic waveguides, we can implement active components such as entangled photon sources on a chip. In this paper, we report recent progress in integrated quantum photonic circuits based on silicon photonics. We review our work on correlated and entangled photon-pair sources on silicon chips, using nanoscale silicon waveguides and silicon photonic crystal waveguides. We also describe an on-chip quantum buffer realized using the slow-light effect in a silicon photonic crystal waveguide. As an approach to combine the merits of different waveguide platforms, a hybrid quantum circuit that integrates a silicon-based photon-pair source and a silica-based arrayed waveguide grating is also presented.

Keywords: integrated quantum photonics; quantum optics; entanglement; silicon photonics; quantum information.

1 Introduction

Optical waveguide technologies have emerged as promising platforms for quantum information processing systems using photons [1–3]. The use of waveguides provides increased phase stability and enables the integration of larger numbers of quantum gates in a limited area. With the use of waveguides, several quantum tasks have been implemented, from basic quantum optic experiments [1, 4, 5] to sophisticated quantum information processing such as Shor's algorithm [6], quantum walks [7, 8], and boson sampling [9–14]. In the future, it is expected that such quantum functional circuits will be integrated on chip with other devices such as photon sources [15, 16], functional circuits [17, 18], buffers [19], and detectors [20–23], so that we can realize all optical quantum processors, as shown in Figure 1 [19].

Silica waveguides were first employed as devices for quantum communication [24–26] and then as a platform for quantum computation [1]. Silica waveguides have been developed as a technology to fabricate devices for optical fiber communication for several decades [27], and thus, the fabrication technology is matured. As a result, the loss per unit length of a typical silica waveguide is currently much smaller than that of waveguides based on other materials. On the other hand, as a typical silica waveguide has a relatively large effective area, the bending radius of a silica waveguide is relatively large (typically larger than a millimeter [28]), leading to a larger device size. In addition, it is relatively difficult to realize an active device based on nonlinear-optical effect, such as a photon-pair source on a silica chip, because of the small nonlinearity of silica waveguides. Note that there have been several reports of photon-pair generation [29–31] using femtosecond laser direct written silica waveguides [32].

With silicon photonics technologies, we can implement a variety of quantum functions on waveguides. One such technology is the silicon wire waveguide (SWW), which is a single-crystal, single-mode silicon waveguide typically about 400 nm wide and 200 nm thick. Because of this small cross-section, together with the large nonlinear refractive index of silicon, we can observe an enhanced nonlinear coefficient γ (/W/m) [33] that is much larger than that of a silica waveguide. Several groups have already reported the generation of correlated [15] and entangled [16] photon pairs using an SWW.

***Corresponding author: Hiroki Takesue,** NTT Basic Research Laboratories, NTT Corporation, 3-1 Morinosato Wakamiya, Atsugi, Kanagawa, 243-0198, Japan, e-mail: takesue.hiroki@lab.ntt.co.jp
Nobuyuki Matsuda: NTT Basic Research Laboratories, NTT Corporation, 3-1 Morinosato Wakamiya, Atsugi, Kanagawa, 243-0198, Japan; and Nanophotonics Center, NTT Corporation, 3-1 Morinosato Wakamiya, Atsugi, Kanagawa, 243-0198, Japan

Edited by Benjamin J. Eggleton and Tara Dorrian

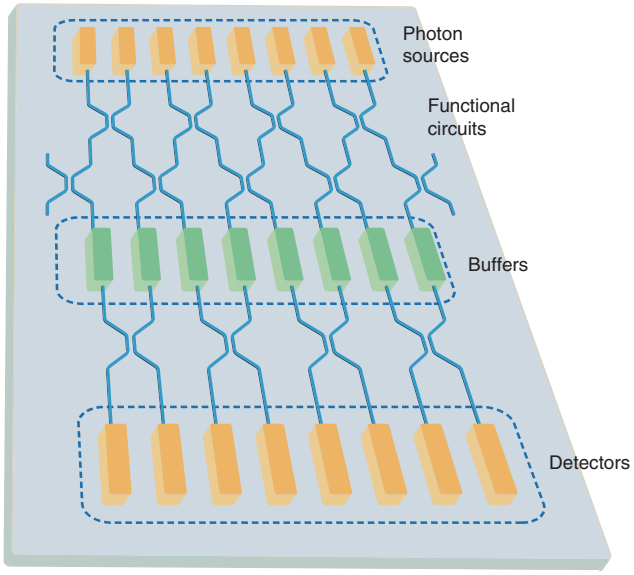

Figure 1: Conceptual diagram of a photonic quantum processor based on integrated quantum photonics.

In this paper, we review the recent progress in integrated quantum photonics based on silicon photonics technologies. Section 2 describes a monolithic polarization entangled photon-pair source on a silicon chip. In Section 3, we describe efforts for realizing ultrasmall correlated and entangled photon-pair sources, based on a silicon photonic crystal (PhC) technology. In Section 4, we introduce a novel function – an on-chip single-photon buffer – realized using PhC technology. We then describe a hybrid approach to integrate active function based on an SWW and a passive function based on a silica waveguide so that we can realize sophisticated photonic quantum information systems. In Section 6, we provide a brief summary.

2 Polarization entangled photon-pair source on a silicon chip

Quantum states of photons can be encoded in polarizations, paths, orbital-angular momentum, frequencies, and temporal positions of light. Of these, a polarization state provides a two-level photonic system, which is easy to manipulate with commercial bulk optics such as waveplates. Hence, it has been at the heart of many quantum information experiments [34–38]. To integrate a polarization-encoded quantum information system on a chip, it is necessary to develop the building blocks, including a polarization entanglement photon-pair source [39, 40]. However, the integration of optical circuits makes handling the polarization slightly more challenging. This is because it is difficult to eliminate the polarization-mode walk-off in a nonlinear waveguide completely [41], which degrades the polarization-encoded quantum states. To compensate for the walk-off, polarization entanglement sources using on-chip waveguides require extra off-chip components [42–46].

We demonstrated the first polarization-entangled photon-pair source fully integrated on a chip as shown in Figure 2 [47]. It consists of two SWW photon-pair sources connected by an ultrasmall silicon polarization rotator [48, 49]. The SWWs have a silicon core that is 400 nm wide, 200 nm high, and 1.5 mm long. The silicon polarization rotator has 30-μm-long off-axis double cores. The inner and outer cores are a silicon wire (200 nm wide and 200 nm high) and a SiO_xN_y waveguide (840 nm wide and 840 nm high), respectively. The SWWs and the polarization rotator are connected by 10-μm-long tapered silicon wires. The undercladdings and overcladdings are SiO_2. For efficient coupling with external optical fibers, both ends of the device are equipped with spot-size converters that are based on an inversed taper structure of the silicon core.

The SWWs and the spot-size converters were fabricated by electron beam lithography and electron cyclotron resonance plasma etching. An 840-nm-thick silicon

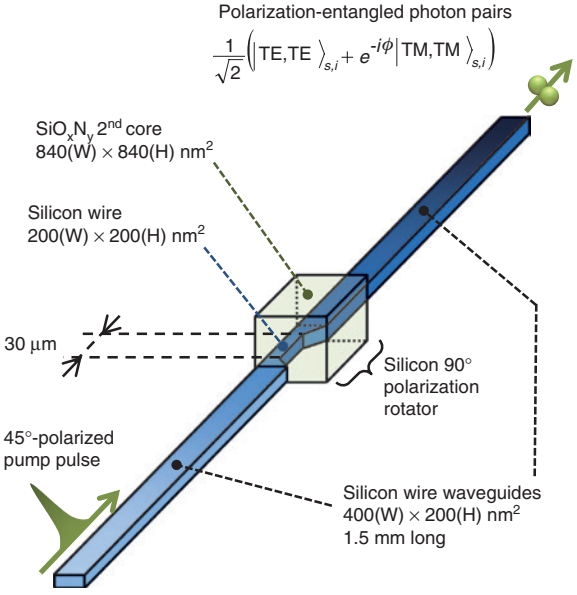

Figure 2: A polarization entangled photon pair source fabricated on a silicon-on-insulator substrate.
The device consists of two silicon wire waveguide photon pair sources and a silicon-wire-based polarization rotator. The silicon substrate and the SiO_2 overcladdings and undercladdings are not shown for clarity [47].

oxynitride film with a refractive index of 1.60 was deposited by the plasma-enhanced chemical vapor deposition, and the second core of the silicon polarization rotator was formed by reactive ion etching with fluoride gas.

In an SWW, a correlated pair of signal and idler photons is created following the annihilation of two pump photons via spontaneous four-wave mixing (FWM) arising from the bound-electronic $\chi^{(3)}$ nonlinearity of the silicon core. Due to the high $\chi^{(3)}$ nonlinearity of silicon in the telecommunication band (e.g. more than 100 times higher than that of silica) and the submicrometer scale mode field diameter [50, 51], correlated photons can be efficiently generated via spontaneous FWM in an SWW [15, 16, 52, 53]. Moreover, the Raman noise photons in a single-crystalline silicon core, which exhibit a sharp spectral peak that is 15.6 THz away from the pump frequency, can be easily eliminated with wavelength filters. Hence, low-noise correlated photons can be efficiently generated in an SWW [54].

Figure 3A shows the wavelength dependence of FWM efficiency in an SWW for cases where the pump, signal, and idler fields are all in the transverse-electric (TE) or transverse-magnetic (TM) mode. We obtained the data via a stimulated FWM experiment [55, 56], where we used two independent wavelength-tunable continuous wave (CW) lasers for the pump and stimulating signal field and observed the overall output spectrum including the generated idler field. Here, the signal wavelength (vertical axis) was scanned while the pump wavelength was fixed. We see that the idler components satisfied the energy conservation of the FWM $2\omega_p=\omega_s+\omega_i$, where $\omega_{p,s,i}$ denotes the frequencies of the pump, signal, and idler fields. Due to a difference in the lateral field confinements and dispersions between the TE and TM modes, the FWM efficiently occurred for the all-TE condition in our SWW.

In the silicon polarization rotator [48], the off-axis double core structure induces two orthogonal eigenmodes with the polarization axis tilted ±45° to the horizon and slightly different refractive indices as shown in Figure 3B. This birefringence provides an on-chip waveplate with fixed birefringence axes. The polarization rotation of a linearly polarized input field depends on the length of the rotator. We used a rotator with a length of 30 μm, which provided a zeroth-order polarization rotation angle of 86.7±0.1° and a polarization extinction ratio exceeding 20 dB for a TE-polarized CW laser at around 1551-nm wavelength [47]. Hence, the rotator served as an on-chip polarization converter between the TE and TM modes, which was the function required for our polarization entanglement source. The insertion loss of the rotator is approximately 1 dB [48].

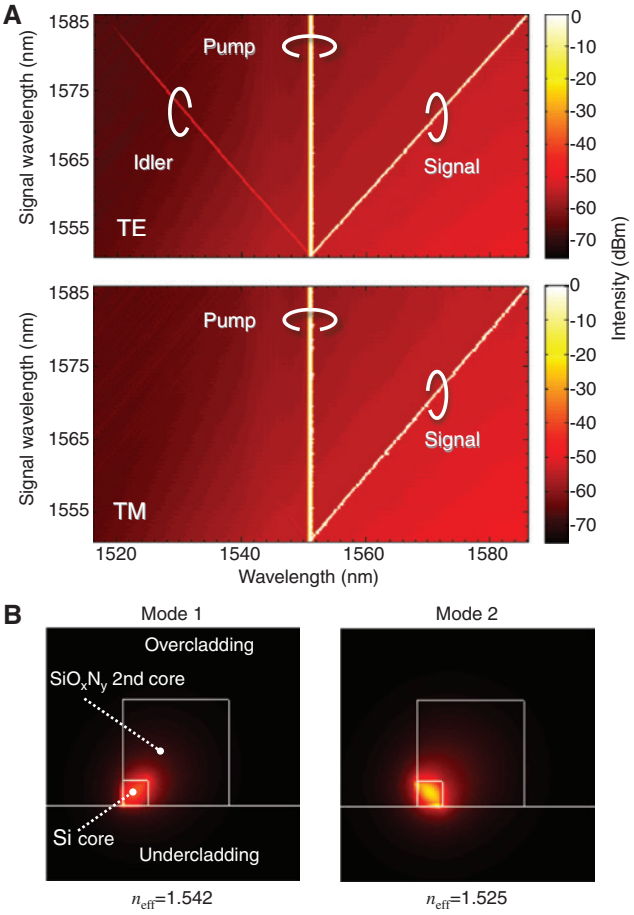

Figure 3: (A) Polarization dependence of the FWM efficiency in an SWW, investigated via stimulated FWM experiment. The density plots show the observed spectrum as a function of the center wavelength of the CW laser used for stimulating signal field. (B) The eigenmodes in the silicon polarization rotator, numerically simulated with a mode solver. Corresponding eigenvalues (effective refractive indices) are also shown. Figures from Ref. [47].

Pump pulses with +45° linear polarization are injected into the polarization entanglement source. Then the input is decomposed into the TE and TM modes in the waveguides. In the first SWW, only the TE-polarized component of the pump pulses creates photon pairs in the TE mode because of the abovementioned polarization dependence. The polarization state of the correlated photons is then converted to the TM mode by the polarization rotator. At the same time, the silicon polarization rotator converts the polarization of TM-polarized pump pulses to TE; these pump pulses create TE-polarized correlated photons in the second SWW. Due to the quantum interference between the photon pairs created in the first and second SWWs, we obtain the following polarization entangled state of photons:

$$|\psi\rangle=\frac{1}{\sqrt{2}}(|\mathrm{TE, TE}\rangle_{s,i}+e^{-i\phi}|\mathrm{TM, TM}\rangle_{s,i}), \quad (1)$$

at the output end of the device. Here, ϕ is a fixed relative phase. The configuration automatically equalizes the two amplitudes and thus provides a maximally entangled state. This is because the reduction of the pairs created in the first SWW from the waveguide loss in the second SWW is equivalent to the reduction of the pairs to be created in the second SWW owing to the loss of the TM component of the input pump pulses in the first SWW [47].

The operation is similar to that of a widely used polarization entanglement source utilizing $\chi^{(2)}$ nonlinear crystals designed for spontaneous parametric down conversion under type I phase matching [40]. The source consists of two nonlinear crystals cascaded with 90° orientation, and horizontally and vertically polarized photon pairs are created in each crystal. In our case, instead of cascading two crystals with 90° orientation, we rotated the polarization between the two SWWs. Thus, the device is designed to be symmetric as regards the polarizations with respect to the midpoint of the device. This structure eliminates the degradation of the output entangled state caused by polarization-dependent walk-offs and losses in the waveguide [47].

The experimental setup is shown in Figure 4A. We input pump pulses with a temporal width of 80 ps and a repetition rate of 100 MHz, obtained by an intensity modulation of a CW laser operated at a wavelength of 1551.1 nm. The polarization of the input pulses was set to be +45° linear polarization. The in-coupled pump peak power was 128 mW. The output signal and idler photons were collected by a lensed fiber and subsequently separated with the wavelength-division-multiplexing filter after they had passed through the notch filters for the pump field rejection. The bandwidth of each channel was 0.14 nm (18 GHz). The time correlated events of the photons were detected with the two InGaAs single-photon avalanche diodes (SPADs) (id210, ID Quantique) and a time-interval analyzer (TIA).

We then performed quantum state tomography on the generated photons [57] by carrying out a polarization-correlation measurement with the polarization analyzers. The reconstructed density matrix ρ of the photons obtained with the maximum-likelihood estimation is shown in Figure 4B. We clearly observed off-diagonal components with amplitudes as high as those of the diagonal components, indicating a high purity of the state. To evaluate the degree of entanglement, we estimated the fully entangled fraction $F(\rho)=\max_{\Psi}\langle\Psi|\rho|\Psi\rangle$, where the maximum is taken over all maximally entangled states

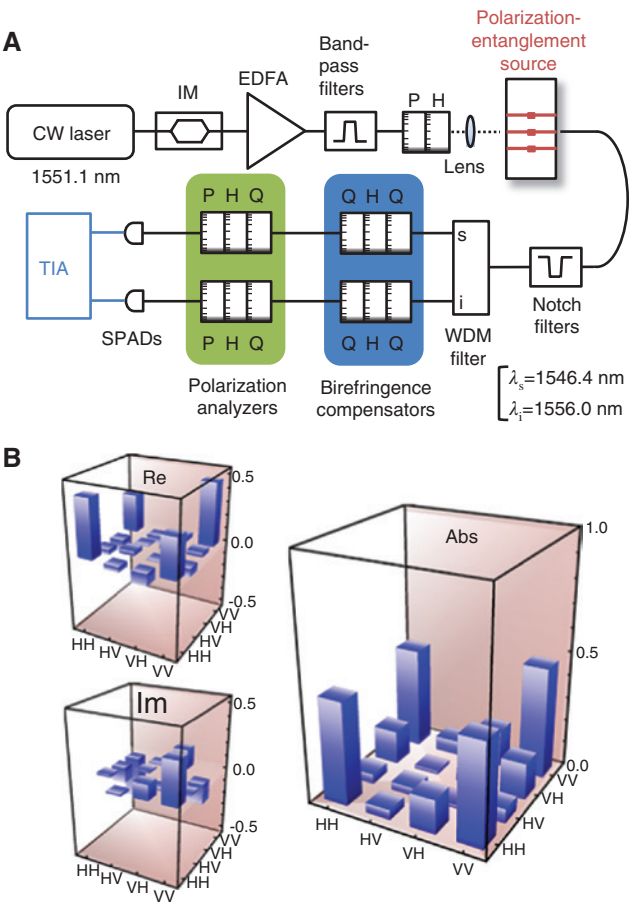

Figure 4: (A) Experimental setup for the measurement of polarization entanglement from the chip. IM: intensity modulator, EDFA: Erbium-doped fiber amplifier, P: polarizer, H: half-wave plate, Q: quarter-wave plate, WDM filter: wavelength-division multiplexing filter. Dashed and solid lines show free-space optical path and electrical connection. (B) The reconstructed density matrix of the two-photon polarization state generated from the chip. H and V represent the TE and TM modes, respectively [47].

$|\Psi\rangle$ [58, 59]. The obtained $F(\rho)=0.91\pm0.02$. Hence, we have successfully generated photons with a high degree of polarization entanglement using the on-chip source. The imperfect fidelity was considered to be mainly due to the wavelength-dependent polarization rotation at the spot-size converters.

Following this work, many researchers demonstrated on-chip polarization entangled sources based on other device architectures and materials. Olislager et al. [60] generated polarization entanglement using two SWWs that were monolithically connected by a two-dimensional (2D) vertical grating coupler. Lv et al. [61] generated polarization entanglement by means of the birefringence of a single SWW. Various polarization entanglement sources based on an $\chi^{(2)}$ nonlinear waveguide made of (Al)GaAs have also been demonstrated [62–66]; these experiments

employing the direct band-gap materials paved the way to the realization of a polarization entanglement source driven by current injection [67, 68]. These results show important steps toward the realization of an integrated quantum information system using the polarizations of light.

In order to realize a polarization-encoded quantum information processor on chip, we need to develop polarization analysis functions, namely the manipulation and projection of polarization states on a chip. Recently, such functions have been achieved using a lithium niobate waveguide modulator [69] and low-birefringence silica waveguides [70–72].

3 Ultrasmall correlated and entangled photon-pair sources using PhC coupled-resonator optical waveguides

We used chip-scale SWWs as a bright and low-noise source of correlated photons. However, further downsizing of the photon source is of great importance in a view to realizing quantum information processing systems with higher integration density. Such integration includes a multiplexed single-photon source [73–76], which was proposed to realize a near-deterministic heralded single-photon source from probabilistic photon-pair sources based on spontaneous parametric processes. The source is a bundle of many identical heralded single-photon sources, each of which generates photon pairs at a low rate (~0.01 pairs/pulse). The whole system provides single photons at a certain period while the multiple pair generation rate is suppressed. This scheme requires many independent photon-pair sources connected with single-photon routing technology. Thus, increasing the integration density of photon-pair sources is required. Another promising approach to realize a near deterministic heralded single-photon source is to employ a temporal multiplexing configuration [77]. This configuration will avoid the size constraints in the spatial multiplexing described above, though at the expense of the reduced repetition frequency of the "triggered" single photons.

A simple solution for further downsizing is to enhance the optical nonlinearity of the photon-pair source per unit size. An effective way to achieve this is to slow down the group velocity of light in a medium v_g [78–81]. This is because the light-matter interaction time can be prolonged by the slow propagation of light. Furthermore, the slow-light mode compresses the optical field longitudinally so that its peak intensity increases, leading to a further enhancement of nonlinearity. Because of these effects, the nonlinear constant γ of an optical waveguide is proportional to n_g^2, where $n_g=c/v_g$ is the group index of the guided mode. Hence, we can significantly increase the nonlinearity and thereby the photon-pair generation rate via the spontaneous FWM ($\propto\gamma^2$) by using the slow light effect.

Slow-light enhancement has been investigated particularly in relation to a silicon photonics platform, where mature nanofabrication technologies allow us to engineer the group velocity of light. Slow-light modes in silicon PhC line defect waveguides [82, 83], and coupled-resonator optical waveguides (CROWs) [84] based on Si microring resonators [85] have been shown to enhance the efficiency of spontaneous FWM. We have demonstrated slow-light enhancement [86] using a CROW consisting of PhC cavities based on mode-gap confinement [87, 88]. The cavity exhibits an ultrahigh Q value and wavelength-sized confinement of light, which enabled us to realize a low-loss and highly nonlinear waveguide. In the following, we review our recent work related to the PhC-based CROW and its application to the photon-pair sources [86, 89–91].

Figure 5 shows a schematic of our CROW fabricated on an air-bridged 2D silicon PhC slab with a triangular lattice of air holes [89]. Lattice constant a is 420 nm, the hole radius is $0.25a$, and the slab thickness is $0.25a$. Each cavity is formed by a local width modulation of a barrier line defect with a width of $0.98\sqrt{3}a$ (W0.98) along the Γ–K direction. The red and green holes are shifted by 8 and 4 nm, respectively, in plane toward the outside. This yields optical cavities with a cavity Q as high as 10^6 and a mode volume of $1.7(\lambda/n)^3$ [87, 88].

In a CROW, the collective resonance of the identical cavities exhibits Bloch modes, whose bandwidth is much larger than that of each cavity linewidth. The mode follows a dispersion relation given by

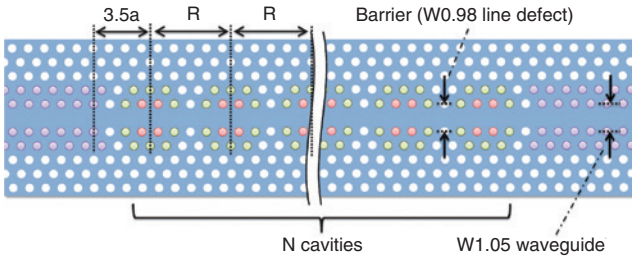

Figure 5: A CROW consisting of photonic-crystal mode gap nanocavities.
The positions of the red and green holes are shifted by 8 and 4 nm toward the outside, respectively [89].

$$\omega=\omega_0(1+\Delta+\kappa_1\cos(KR)) \quad (2)$$

under the tight-binding approximation [84]. Here, κ_1 is nearest neighbor coupling strength between cavities, ω_0 is the center frequency of each cavity, Δ is the center frequency offset of the band from ω_0, and R is cavity pitch. This band formation for photons is analogous to electronic band formation of atoms in a crystal lattice. The bandwidth of the supermode is $2\omega_0\kappa_1$, and at center frequency $\omega=\omega_0$, the group-velocity dispersion is zero and the group velocity becomes $v_g=\frac{d\omega}{dK}=\omega_0\kappa_1 R$. Thus, we can control v_g by designing κ_1 and R. CROWs consisting of more than a 100 resonators have been developed using short waveguide elements [92], microring resonators [93, 94], microdisk resonators [95], and PhC cavities [87]. So far, a v_g value as small as $c/170$ for an optical pulse has been realized using a PhC-based CROW [87].

To couple the light to our CROW, access waveguides consisting of W1.05 line-defect waveguides and SWWs (not shown) were fabricated. Intercavity distance was apodized at the CROW-waveguide connection. Reference waveguides, where the CROW section was replaced with a W1.05 line defect waveguide, were also fabricated on the same chip. The reference waveguide had n_g~5.

Figure 6A shows linear transmission spectra of the CROWs (with $R=5a$ and cavity number N=200 and 400) and the reference waveguide, measured with a wavelength-tunable CW laser at TE polarization [89]. Each CROW exhibited a clear passband with isolations of over 30 dB. The loss comprised fiber-waveguide coupling loss (-8 dB/facet), waveguide propagation loss (-2 dB/mm), and additional loss at waveguide-CROW connections (-1 dB/facet).

The CROW with N=200 exhibited a transmission bandwidth of 6 nm, from which κ_1 was estimated to be 1.9×10^{-3} from Eq. (2). The value agreed well with that obtained from CROWs with smaller N (5 and 10) [87]. This indicated that the slow-light mode was extended toward the region over 100 cavities, where it was less influenced by structural fluctuation due to fabrication error. A statistical analysis [96, 97] revealed that the light transport in our CROW is less relevant than in a localized or diffusive transport regime [89]. On the other hand, we saw a decrease in the transmission bandwidth for N=400. This was because of degradation of the light transport characteristics, which was also indicated by the statistical analysis in the corresponding wavelength region [89]. However, the signature of the ballistic transport held in the wavelength region surrounded by the dashed lines in Figure 6A, where we could observe slow-light

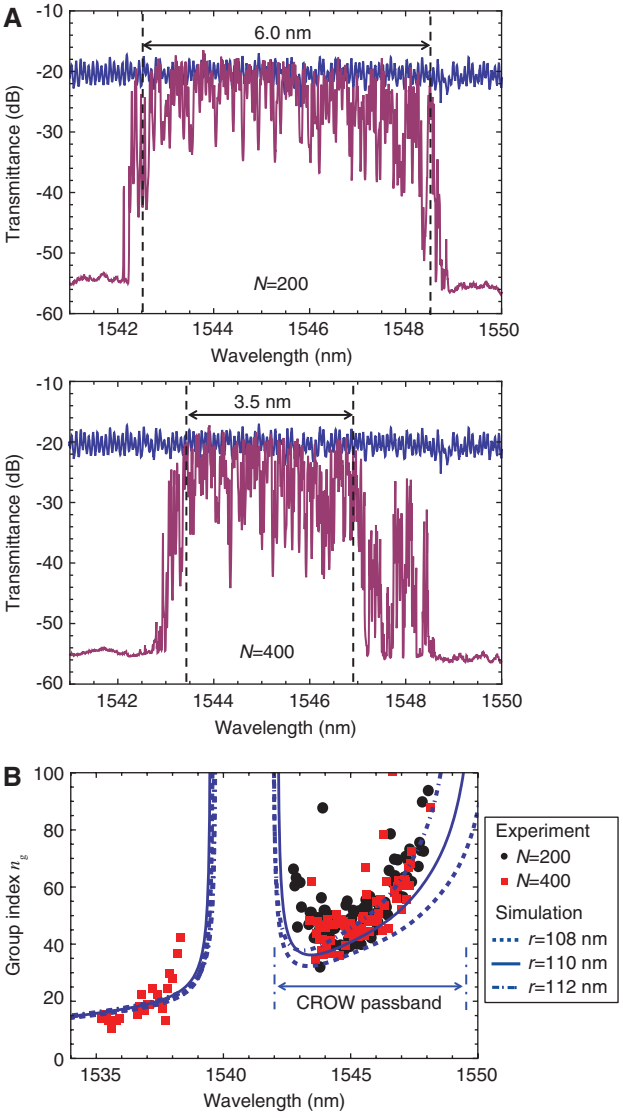

Figure 6: (A) Transmission spectra of CROWs (red curves) and a W1.05 line-defect waveguide (blue curves). (B) Measured group index spectra for CROWs with various cavity numbers along with the numerical simulation results based on the plane-wave expansion method. Figures from Ref. [89].

propagation without significant pulse distortion [19] (see Section 4).

The dispersion properties of the CROWs were investigated with the pulsed time-of-flight method [89]. Plots in Figure 6B show the measured n_g spectra. The data were extracted from the transit time difference of optical pulses (duration: 80 ps) between the CROWs and the reference waveguides. A slow-light mode with n_g~40 was obtained at around the band center. In addition, the n_g values were independent of the cavity number N as expected.

However, the dispersion curve was asymmetric with respect to the center of the CROW passband, distinct from

the shape given by Eq. (2). This is because the tight-biding model assumes that the resonator eigenmodes are nondispersive. In our case, the cavity confinement was based on the modulation of the line defect, whose mode exhibited dispersion. In fact, v_g at the band center was estimated to be $c/65$ from Eq. (2), which is distinct from the observed value at around the band center. Lian et al. [98] explained this by introducing an energy dependence in κ_1. Another reason for the discrepancy is the effect of the next-nearest-neighbor coupling between cavities, which was investigated by Caselli et al. [99].

To confirm that the observed modes were induced by our CROW structure shown in Figure 5, we performed a numerical simulation of the dispersion, namely, the photonic band structure, with a three-dimensional vector plane-wave expansion method using BandSOLVE (Synopsys, Inc., Mountain View, CA USA) [89]. The results are shown as curves in Figure 6B. The numerical results showed good agreement with the experimental data, including the asymmetric shape. The mode at the wavelength region shorter than the minigap at around 1540 nm appeared due to the band folding of the original line-defect mode at the CROW periodicity of $R=5a$. This also well explained the experimental data.

Using the CROW, we investigated the slow-light enhancement of $\chi^{(3)}$ nonlinearity for the correlated photon-pair generation [86]. In doing so, we performed the stimulated FWM experiment as described in Section 2. The observed FWM spectra are shown as a density plot in Figure 7. The pump and signal powers coupled to the waveguides were 1.6 and 0.5 mW, respectively. In both cases, we observed the idler wavelength component satisfying the energy conservation of the FWM. However, the CROW exhibited the brighter idler peaks, thanks to the slow-light-enhanced nonlinearity. From the result, we estimated nonlinear constant γ of the CROW to be 7200/W/m at $n_g=36$ and 13,000/W/m at $n_g=49$. These values are much larger than that of an SWW (typically 200–300/W/m). Indeed, this is the first experimental observation of a γ value exceeding 10,000/W/m in a silicon-core nonlinear waveguide. Note that we used a CROW sample different from the one used in the stimulated FWM experiment above (but with the same specifications).

Next, we undertook the photon-pair generation experiment via the spontaneous FWM in our CROW [90]. Figure 8A shows the experimental setup. We obtained pump pulses centered at 1545.4 nm with a pulse duration of 130 ps and repetition rate of 100 MHz using a setup similar to that shown in Figure 4A. The output pulses containing correlated photons were collected with a lensed fiber. Notch filters with a suppression bandwidth of

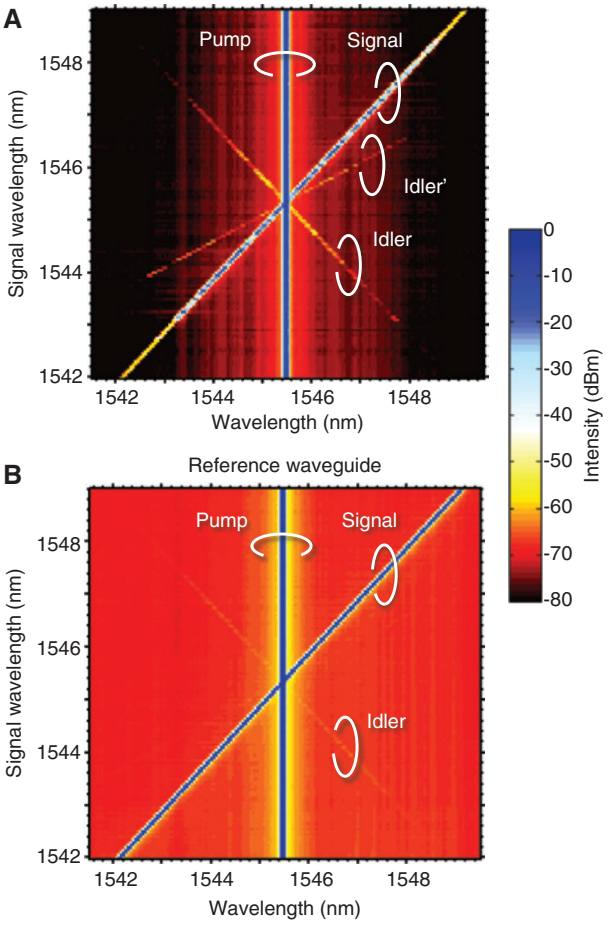

Figure 7: Stimulated FWM spectra using (A) the CROW with $N=200$ and (B) the W1.05 reference waveguide.
The line labeled Idler' in (A) was generated as a result of frequency conversion of the "pump" via FWM pumped by the "signal" [86].

1.0 nm centered at the pump wavelength were introduced for the pump field rejection. Then, the photon pairs were separated by the arrayed waveguide grating (AWG) into different fiber channels with a transmission bandwidth of 0.2 nm (25 GHz). The pump-to-signal (or -idler) detuning was chosen to be 0.8 nm, which was within the FWM bandwidth as seen in Figure 7A. After further noise suppression, the photons were received by the single photon counting modules (SPCMs), and their temporal correlation was analyzed by the TIA. The overall transmittance of the filtration system was approximately -6 dB, while the transmittance at the pump wavelength was <-130 dB.

Figure 8B shows the estimated photon-pair rate at the output ends of the waveguides as a function of the in-coupled average power of the pump pulses. The measurement time was 120 s for each data point for good statistics. We were able to successfully observe the slow-light enhancement of the photon-pair generation rate in our CROW. Indeed, the generation rate was almost two orders of

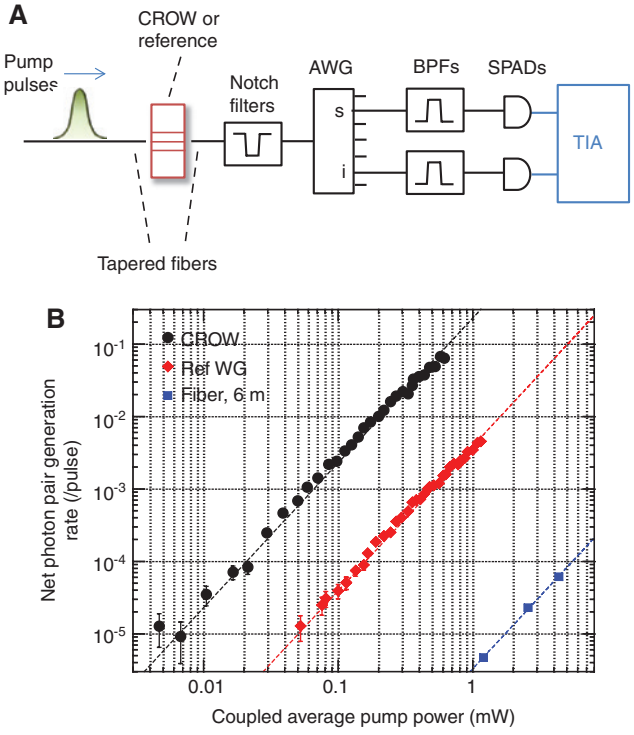

Figure 8: (A) Experimental setup for correlated photon pair generation from the CROW. AWG: arrayed-waveguide grating. (B) Net photon pair generation rate from various waveguides as a function of the in-coupled average pump power. Dashed lines represent fitting results using Eq. (3) [90].

magnitude larger than that with the reference line-defect waveguide. The photon-pair generation in 6-m fiber links for the measurement was negligible.

Under the slowly varying envelope approximation, we obtain the photon-pair generation rate per pump pulse μ_c via spontaneous FWM as

$$\mu_c = \Delta\nu\Delta t(\gamma P_{peak} L_{eff})^2 \tag{3}$$

when the pump-to-signal (or -idler) detuning is within the FWM bandwidth, where $\Delta\nu$ is the bandwidth of the wavelength filters for the signal and idler channels, Δt is the temporal width of the pump pulses, and P_{peak} is the pump peak power. L_{eff} is the loss-averaged effective waveguide length associated with $L_{eff}=(1-e^{-\alpha L})/\alpha$, where α is the attenuation coefficient.

The dashed lines in Figure 8B show the fittings using Eq. (3). One can see that the experimental data exhibited good power-squared dependence. From the fitted function for the CROW, we obtained a γ of 9000/W/m, which was in good agreement with that obtained via the stimulated FWM experiment. This value was ~30 times larger than that of standard SWWs [53]. In other words, the photon-pair generation rate of our CROW was 10^3 times larger than in an SWW per unit length.

We also verified the nonclassicality of the photon pairs from the CROW by testing the violation of the Zou-Wang-Mandel inequality, which is valid for classical correlation [100]. We have successfully demonstrated the violation by 20 standard deviations. Hence, we confirmed the generation of nonclassical photon pairs from the CROW based on the PhC nanocavities [90].

Furthermore, we have demonstrated the generation of time-bin entangled photons from the CROW [91]. The experimental setup is shown in Figure 9A. A 60-ps, 1-GHz clock coherent pulse train with a wavelength of 1545.5 nm was launched into the CROW with N=200. Through the slow-light enhanced SFWM in the CROW, we generated high-dimensional time-bin entangled photon pairs whose state is given by

$$|\Psi\rangle = \sum_{k=1}^{N_c} |k\rangle_s |k\rangle_i, \tag{4}$$

where N_c is the number of pump pulses where coherence is preserved and $|k\rangle_x$ denotes a quantum state where a single photon is at the kth temporal slot in mode x (=s: signal, i: idler). The photons from the CROW were passed through filters similar to the ones in Figure 8A and launched into 1-bit delayed Mach-Zehnder interferometers for Franson

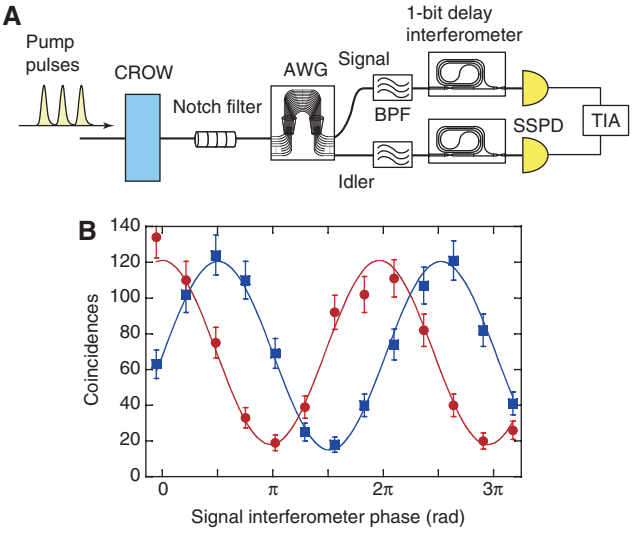

Figure 9: Time-bin entangled photon-pair generation using the CROW.
(A) Experimental setup. SSPD: superconducting single-photon detector. The wavelengths of the signal and idler channels were 1544.6 and 1546.2 nm, respectively. The photon bandwidth was 0.1 nm, limited by the bandwidth of the AWG. (B) Two-photon interference fringes. Squares: idler interferometer phase at 0, circles: $\pi/2$.

interferometry measurement [101]. The obtained two-photon interference fringes are shown in Figure 9B, where we observed clear sinusoidal modulations of coincidences for two nonorthogonal measurement bases for the idler photons. The visibilities of the fringes were 78.0±3.9% (idler interferometer phase 0) and 74.1±4.8 ($\pi/2$), which indicates that we obtained an entangled state that can violate Bell's inequality. This was the first observation of quantum entanglement generated from a slow-light waveguide.

4 On-chip quantum buffer

In the photonic quantum circuit shown in Figure 1, synchronization of photons at functional circuits is crucial for obtaining quantum interference. Such integration becomes more difficult as the integration density increases and the circuits are further scaled down. A buffer can store a photon for a certain amount of time so that we can adjust the arrival time of a photon at each circuit. Inclusion of such a buffer enables a flexible circuit design. In addition, we may be able to realize a fully programmable integrated quantum optical circuit if we use a tunable buffer together with other active elements such as optical switches.

We can realize an integrated single-photon buffer by using the slow-light effect in optical waveguides [79, 80, 93]. We demonstrated a single-photon buffer on a silicon chip using the PhC-based CROW with the number of cavities N=400 (inset of Figure 10) [19]. The total length of the CROW was 840 μm. A 10-μm PhC line-defect waveguide was placed at each end of the CROW. The transmission spectrum of the CROW moved to longer wavelength as we increased the chip temperature, and the dependence was measured to be ~0.07 nm/°C.

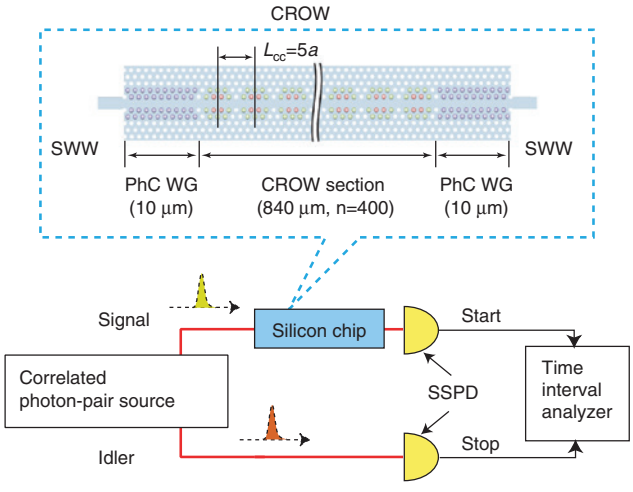

Figure 10: Setup for observing photon buffering. Inset: CROW consisting of PhC nanocavities.

The experimental setup for observing photon buffering is shown in Figure 10. A photon-pair source based on spontaneous FWM in a dispersion shifted fiber emitted photon pairs whose wavelengths were 1546.7 (signal) and 1555.53 (idler) nm. The bandwidth of the photons was 0.2 nm. The signal photon was coupled to the silicon chip that included the CROW and the reference waveguide using lensed fibers. The reference waveguide (the W1.05 line defect) was used as the temporal reference when measuring the delay caused by the CROW. The signal photons outputs from the chip were received by a superconducting single-photon detector (SSPD), while the idler photons were directly detected by a second SSPD. The detection signals from the SSPDs were input into a time interval analyzer as the start and stop signals, respectively.

Figure 11A and B shows the histograms obtained in the time interval analysis. We observed the largest peaks at the relative delay near 0, which correspond to the coincidences caused by the signal and idler photons that form correlated pairs. From these data, the cross-correlation $g_{si}^{(2)}(0)=P_{si}/P_sP_i$ [P_{si}: coincidence detection probability, P_s (P_i): signal (idler) photon detection probability], with which we can quantify the strength of intensity correlation between photons [102], was obtained as 3.25±0.06 for the CROW and 3.10±0.05 for the reference waveguide. Note that $g_{si}^{(2)}(0)>2$ implies the existence of nonclassical intensity correlation [102]. The cross-correlation value was 3.22±0.05 when we removed the chip, suggesting that the nonclassical intensity correlation was preserved even after the single photon had travelled through as many as 400 high-Q nanocavities without any degradation.

The coincidences at the main peaks correspond to the temporally resolved detection events of the single photons heralded by the detection of idler photons. Thus, we could measure the delay time of the signal photons in the CROW by observing the temporal shift of the main peaks. An enlarged image of the main peaks in Figure 11A and B is shown in Figure 11C, where we can observe a clear separation of the two peaks. This result shows that the CROW stored the single photon for 151.1±0.5 ps. The group index n_g of the reference waveguide was ~5, which means that the speed of the pulsed photon in the CROW was decreased to 1/59 of the light speed in a vacuum.

We can also tune the buffer time with the CROW. As stated above, the transmission spectrum of the CROW moved as we changed the chip temperature. This implies that we can shift the dispersion characteristic of the

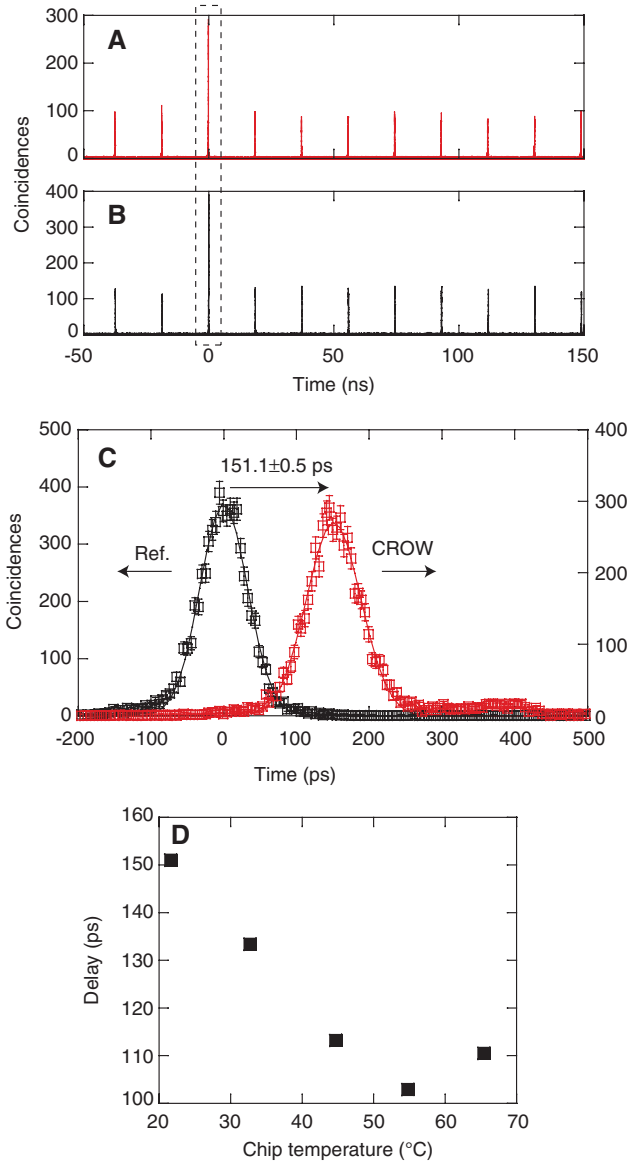

Figure 11: On-chip buffer experimental results.
(A, B) Time interval histograms when the signal photons passed through the (A) CROW and (B) reference waveguide. (C) Enlarged main peaks observed in dashed box in (A) and (B). The red and black squares show the histograms obtained with the CROW and the reference waveguide, respectively. (D) Delay caused by the CROW as a function of chip temperature [19].

CROW by changing the temperature. In fact, we observed a change in the delay time when varying the chip temperature in a measurement similar to the one from which we obtained the data shown in Figure 11C. The experimentally obtained delay time as a function of the chip temperature is shown in Figure 11D. Thus, we could tune the buffer time by ~50 ps with a waveguide as short as 840 μm. Note that we need 1.5-cm variable delay for 50-ps tunability in free space.

5 Silicon-silica hybrid waveguide platform for integrated quantum photonics

As we discussed so far, intensive studies are under way with the aim of developing on-chip quantum information devices, such as the processor shown in Figure 1. To fully exploit the advantages of integrated photonics, it would be ideal to integrate these different components on a single substrate. Motivated by this, many researchers have recently demonstrated the hybrid integration of different quantum-optical components [103–109]. Hence, the stage of integrated quantum photonics research is now moving to hybrid integration on a chip.

Among the building blocks, quantum circuits can be realized by using integrated waveguides with cores made of silicon [18, 108, 110], GaAs [111], or silica-based materials [1, 10, 13, 112]. Of these approaches, silica-based waveguide technology has realized planar lightwave circuits with a significantly large scale for classical optical communication [113, 114]; this capability will facilitate the construction of large-scale quantum circuits. In this context, a research group including an author of this paper has recently realized a silica-based universal linear optical circuit, which is capable of implementing any unitary operations to path-encoded quantum states with full reprogrammability [17]. In addition, the low nonlinearity of silica [115] helps in avoiding the generation of unwanted photons by the intense pump fields used for photon-pair generation in quantum light sources. To exploit these advantages, integrating quantum light sources and silica waveguides is an attractive approach for constructing on-chip quantum information systems.

As stated above, silicon waveguides are useful as photon-pair sources. To incorporate the advantage of silicon with that of silica-based quantum circuits, we have realized a silicon-silica monolithic integration platform as shown in Figure 12 [116]. The platform consists of a silicon and silicon-rich silica (SiO_x) waveguides that are adiabatically interconnected with spot-size converters [117, 118]. The SiO_x waveguides have a core-cladding index contrast of ~3%. The coupling loss at the spot-size converter interface is as small as -0.35 dB per connection [119].

We investigated the photon-pair generation property of the silicon-silica monolithic waveguide platform. From experiments using waveguides with various lengths, we confirmed that most of the photon pairs were generated in the silicon waveguide region. Hence, the contribution of our silica-based waveguide to unnecessary photon generation was negligible as expected. Furthermore, the

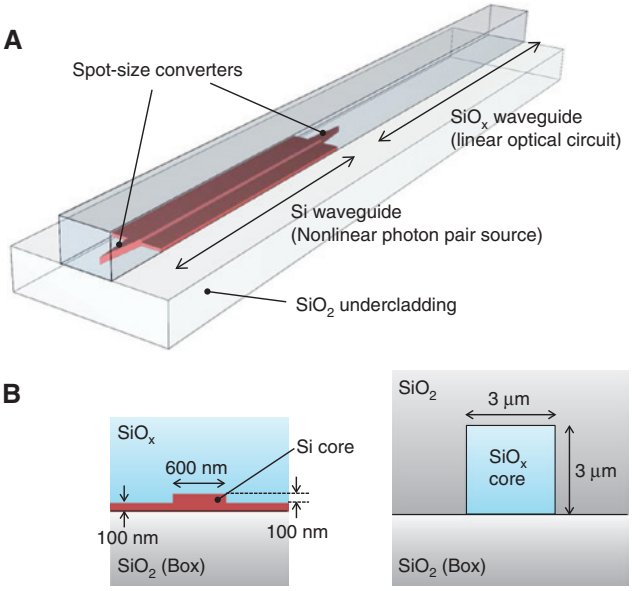

Figure 12: (A) Silicon-silica monolithic waveguide platform for integrating photonic quantum information devices. The silica overcladding and silicon substrate are not displayed for clarity. (B) Cross-sectional views of each waveguide section [116].

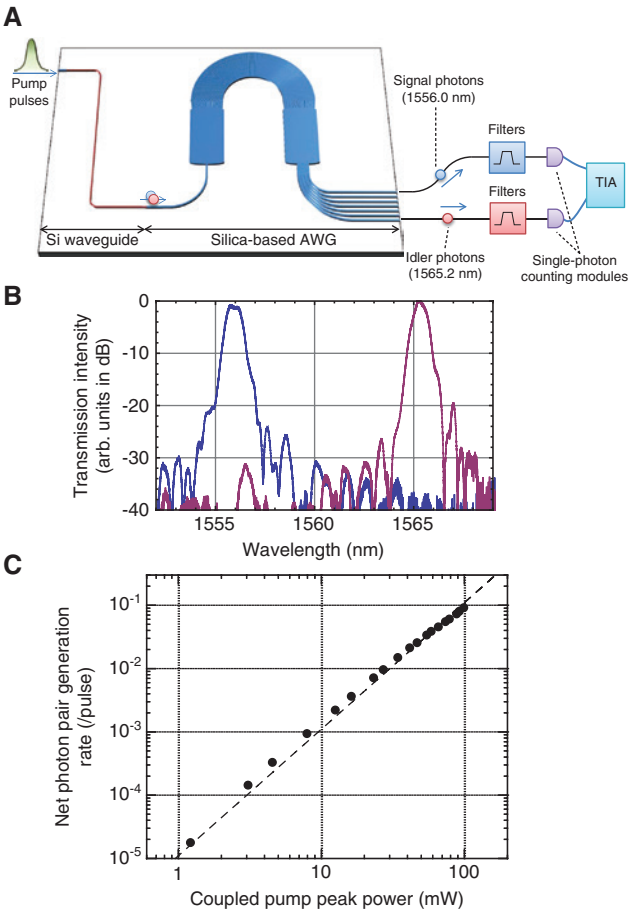

Figure 13: (A) A chip housing a silicon waveguide photon pair source and a silica-based AWG, illustrated with the experimental setup. (B) Transmission spectra from the on-chip AWG output ports used for the collection of the photon pairs. (C) Net photon pair generation rate as a function of pump peak power [116].

nonlinearity of the silicon waveguide γ was estimated to be 161/W/m, which is as high as that of silicon waveguides fabricated without the SiO_x deposition process [53].

Toward full-scale integration, an important step is the integration of a photon-pair source with its interface, namely, a photon-pair demultiplexer. Using the monolithic platform, we constructed a chip capable of generating and demultiplexing quantum correlated photons [89]. Figure 13A is a schematic diagram of the monolithic device together with the experimental setup. In the device, correlated photon pairs were created via spontaneous FWM in an SWW with a length of 1.37 cm and subsequently spectrally separated by the on-chip SiO_x AWG into different output channels. The AWG had 16 output channels designed to have a 200-GHz channel spacing.

In the experiment, we obtained pump pulses centered at 1560.5 nm with a pulse duration of 200 ps and repetition rate of 100 MHz using a setup similar to that shown in Figure 4A. Photons were collected from a pair of waveguides that were three channels away from the center output port. The transmission spectra of the two AWG outputs are shown in Figure 13B. The 3-dB passband widths of the transmission windows are approximately 80 GHz. The spot-size converter interfaced the silicon waveguide and the AWG. The output optical fields were collected by optical fibers with a high numerical aperture integrated on a V-groove array. Then the photons were introduced into spectral filters, each of which consisted of a fiber-Bragg-grating notch filter and a band-pass filter (BPF) for the suppression of residual pump fields. The 3-dB bandwidth of the BPF $\Delta\nu$ was 100 GHz, which covered the AWG passbands. The photons were received by InGaAs SPADs and a coincidence measurement was performed. The overall transmittance of the filters was -2.8 dB and the AWG insertion loss was -7.7 dB.

Figure 13C shows the net photon-pair generation rate estimated from the experiment as a function of the pump peak power. The data exhibited good power-squared dependence, indicating photon-pair generation via the spontaneous FWM process. The solid line shows the estimation obtained with Eq. (3) using the same γ=161/W/m obtained above and the insertion loss of the AWG. The experimental result agreed well with the calculation.

The chip can be used as a compact correlated photon pair source and will be useful for the construction of a multiplexed single-photon source [103] and for

wavelength-division multiplexing quantum communication technologies [120]. The silica-based AWG can provide an interface between a silicon-based photon pair source and silica-based functional circuits [17]. The wavelength-multiplexing capability would be useful for harnessing high-dimensional quantum states on a chip [121, 122]. An integration with high-speed optical switches using a silicon-$LiNbO_3$ hybrid integration approach is attractive for realizing a quantum information system with further functionality [123].

6 Summary and discussion

We have reviewed the recent progress in integrated quantum photonics based on silicon photonics technologies. We have described a monolithic integration of a polarization entangled photon pair source based on an SWW as an example of a quantum optical circuit that integrates several optical devices to realize a quantum function. We have also described our efforts to develop ultracompact photon sources based on silicon PhC technologies, which will be useful for realizing an on-demand single-photon source based on the heralding approach. As a novel function that will be useful for flexible design of integrated quantum optical circuits, we have presented an experiment on an integrated quantum buffer realized with silicon PhC. Finally, we have shown a hybrid approach, with which we can combine the advantages of silica and silicon platforms.

We have developed both polarization and time-bin entangled photon-pair sources. An advantage of polarization qubits is that we can utilize schemes developed in previous free-space quantum information experiments, including various quantum gates based on polarization beam splitters. On the other hand, the majority of waveguide devices show polarization-dependent loss and dispersion, which makes it relatively challenging to build a large-scale system based on polarization qubits. Time-bin qubits are potentially useful for waveguides with polarization dependence, but they have not been studied intensively for complex quantum information experiments. Thus, further investigations to develop various functional circuits based on time-bin qubits are needed. As such an investigation, a two-qubit operation of time-bin qubits has been demonstrated using an optical switch based on a lithium niobate waveguide [124].

The topics introduced here are the basic elements for a photonic quantum system on silicon chips. Therefore, an important future work is to integrate these elements. It is relatively straightforward to combine SWWs and silicon PhC waveguides on the same chip, and in fact, our CROWs are integrated with SWWs. The use of the hybrid integration described in Section 5 enables us to combine low-loss functional circuits based on silica waveguides with other functions realized on silicon waveguides, including the SWWs and PhC waveguides. The choice of elements depends on the purpose of the system. For example, the polarization entangled photon-pair source introduced in Section 2 will be useful for realizing polarization-qubit-based quantum systems on chips, while ultra-small photon-pair sources based on CROW are advantageous for larger scale quantum systems based on path or time-bin encoding. In addition, it is also possible to use the CROW for systems based on the polarization encoding by incorporating the polarization diversity technique reported in Ref. [49]. When integrated with the various functional circuits and on-chip detectors developed so far, we expect that the technologies shown here will contribute to the realization of quantum processors based on fully integrated quantum optical circuits.

Acknowledgments: The authors thank K. Yamada, T. Tsuchizawa, H. Fukuda, T. Watanabe, H. Nishi, E. Kuramochi, H. Taniyama, M. Notomi, H. Le Jeannic, P. Karkus, W.J. Munro, K. Shimizu, and Y. Tokura for their collaborations. The work presented here was supported in part by a Grant-in-Aid for Scientific Research (No. 22360034) from the Japan Society for the Promotion of Science.

References

[1] Politi A, Cryan MJ, Rarity JG, Yu S, O'Brien JL. Silica-on-silicon waveguide quantum circuits. Science 2008;320:646–9.
[2] O'Brien JL, Furusawa A, Vučkovićć J. Photonic quantum technologies. Nat Photon 2009;3:687–95.
[3] Ladd TD, Jelezko F, Laflamme R, Nakamura Y, Monroe C, O'Brien JL. Quantum computers. Nature 2010;464:45–53.
[4] Metcalf BJ, Thomas-Peter N, Spring JB, Kundys D, Broome MA, Humphreys PC, Jin X-M, Barbieri M, Kolthammer WS, Gates JC, Smith BJ, Langford NK, Smith PGR, Walmsley IA. Multiphoton quantum interference in a multiport integrated photonic device. Nat Commun 2013;4:1356.
[5] Matthews JCF, Politi A, Stefanov A, OBrien JL. Manipulation of multiphoton entanglement in waveguide quantum circuits. Nat Photon 2009;3:346E50.
[6] Politi A, Matthews JCF, OBrien JL. Shorâs quantum factoring algorithm on a photonic chip. Science 2009;325:1221.
[7] Peruzzo A, Lobino M, Matthews JCF, Matsuda N, Politi A, Poulios K, Zhou X-Q, Lahini Y, Ismail N, Wörhoff K, Bromberg Y, Silberberg Y, Thompson MG, O'Brien JL. Quantum walks of correlated photons. Science 2010;329:1500–3.

[8] Crespi A, Osellame R, Ramponi R, Giovannetti V, Fazio R, Sansoni L, De Nicola F, Sciarrino F, Mataloni P. Anderson localization of entangled photons in an integrated quantum walk. Nat Photon 2013;7:322–8.
[9] Broome MA, Fedrizzi A, Rahimi-Keshari S, Dove J, Aaronson S, Ralph TC, White AG. Photonic boson sampling in a tunable circuit. Science 2013;339:794–8.
[10] Spring JB, Metcalf BJ, Humphreys PC, Kolthammer WS, Jin X-M, Barbieri M, Datta A, Thomas-Peter N, Langford NK, Kundys D, Gates JC, Smith BJ, Smith PGR, Walmsley IA. Boson sampling on a photonic chip. Science 2013;339:798–801.
[11] Tillmann M, Dakić B, Heilmann R, Nolte S, Szameit A, Walther P. Experimental boson sampling. Nat Photon 2013;7:540–4.
[12] Crespi A, Osellame R, Ramponi R, Brod DJ, Galvão EF, Spagnolo N, Vitelli C, Maiorino E, Mataloni P, Sciarrino F. Integrated multimode interferometers with arbitrary designs for photonic boson sampling. Nat Photon 2013;7:545–9.
[13] Spagnolo N, Vitelli C, Bentivegna M, Brod DJ, Crespi A, Flamini F, Giacomini S, Milani G, Ramponi R, Mataloni P, Osellame R, Galvão EF, Sciarrino F. Experimental validation of photonic boson sampling. Nat Photon 2014;8:615–20.
[14] Bentivegna M, Spagnolo N, Vitelli C, Flamini F, Viggianiello N, Latmiral L, Mataloni P, Brod DJ, Galvão EF, Crespi A, Ramponi R, Osellame R, Sciarrino F. Experimental scattershot boson sampling. Sci Adv 2015;1:3.
[15] Sharping JE, Lee KF, Foster MA, Turner AC, Schmidt BS, Lipson M, Gaeta AL, Kumar P. Generation of correlated photons in nanoscale silicon waveguide quantum circuits. Opt Express 2006;14:12388–93.
[16] Takesue H, Tokura Y, Fukuda H, Tsuchizawa T, Watanabe T, Yamada K, Itabashi S. Entanglement generation using silicon wire waveguide. Appl Phys Lett 2007;91:201108.
[17] Carolan L, Harrold C, Sparrow C, Martín-López E, Russell NJ, Silverstone JW, Shadbolt PJ, Matsuda N, Oguma M, Itoh M, Marshall GD, Thompson MG, Matthews JCF, Hashimoto T, O'Brien JL, Laing A. Universal linear optics. Science 2015;349:711.
[18] Harris NC, Steinbrecher GR, Mower J, Lahini Y, Prabhu M, Baehr-Jones T, Hochberg M, Lloyd S, Englund D. Bosonic transport simulations in a large-scale programmable nanophotonic processor. arxiv:1507.06406 [quant-ph].
[19] Takesue H, Matsuda N, Kuramochi E, Munro WJ, Notomi M. An on-chip coupled resonator optical waveguide single-photon buffer. Nat Comm 2013;4:2725.
[20] Sprengers JP, Gaggero A, Sahin D, Jahanmirinejad S, Frucci G, Mattioli F, Leoni R, Beetz J, Lermer M, Kamp M, Höfling S, Sanjines R, Fiore A. Waveguide superconducting single-photon detectors for integrated quantum photonic circuits. Appl Phys Lett 2011;99:18110.
[21] Pernice WH, Schuck C, Minaeva O, Li M, Goltsman GN, Sergienko AV, Tang HX. High-speed and high-efficiency travelling wave single-photon detectors embedded in nanophotonic circuits. Nat Commun 2012;3:1325.
[22] Sahin D, Gaggero A, Zhou Z, Jahanmirinejad S, Mattioli F, Leoni R, Beetz J, Lermer M, Kamp M, Höfling S, Fiore A. Waveguide photon-number-resolving detectors for quantum photonic integrated circuits. Appl Phys Lett 2013;103:111116.
[23] Najafi F, Mower J, Harris N, Bellei F, Dane A, Lee C, Kharel P, Marsili F, Assefa S, Berggren KK, Englund D. On-chip detection of non-classical light by scalable integration of single-photon detectors. Nat Commun 2015;6:5873.
[24] Honjo T, Inoue K, Takahashi H. Differential-phase-shift quantum key distribution experiment with a planar light-wave circuit Mach-Zehnder interferometer. Opt Lett 2004;29:2797–9.
[25] Nambu Y, Hatanaka T, Nakamura K. BB84 quantum key distribution system based on silica-based planar lightwave circuits. Jpn J Appl Phys 2004;43:L1109–10.
[26] Takesue H, Inoue K. Generation of 1.5-μm band time-bin entanglement using spontaneous fiber four-wave mixing and planar lightwave circuit interferometers. Phys Rev A 2005;72:041804(R).
[27] Kawachi M. Silica waveguides on silicon and their application to integrated-optic components. Opt Quantum Electron 1990;22:391E16.
[28] Takahashi H. High performance planar lightwave circuit devices for large capacity transmission. Opt Express 2011;19:B173–80.
[29] Spring JB, Salter PS, Metcalf BJ, Humphreys PC, Moore M, Thomas-Peter N, Barbieri M, Jin X-M, Langford NK, Steven Kolthammer W, Booth MJ, Walmsley IA. On-chip low loss heralded source of pure single photons. Opt Express 2013;21:13522.
[30] Spring JB, Salter P, Mennea P, Metcalf B, Humphreys PC, Moore M, Gates JC, Thomsa-Peter N, Barbieri M, Jin X-M, Langford NK, Kolthammer SW, Smith PG, Booth M, Smith BJ, Walmsley IA. Quantum interference of multiple on-chip heralded sources of pure single photons. Quantum Information and Measurements 2014, paper QW1B, 2014.
[31] Yan Z, Duan Y, Helt LG, Ams M, Withford MJ, Steel MJ. Generation of heralded single photons beyond 1100 nm by spontaneous four-wave mixing in a damage-stressed femtosecond laser written waveguide. Appl Phys Lett 2015;107:231106.
[32] Psaila ND, Thomson RR, Bookey HT, Shen S, Chiodo N, Osellame R, Cerullo G, Jha A, Kar AK. Supercontinuum generation in an ultrafast laser inscribed chalcogenide glass waveguide. Opt Express 2007;15:15776–81.
[33] Agrawal GP, Nonlinear fiber optics, 3rd ed. Academic, 2011.
[34] Gisin N, Ribordy G, Tittel W, Zbinden H. Quantum cryptography. Rev Mod Phys 2002;74:145–95.
[35] Knill E, Laflamme R, Milburn GJ. A scheme for efficient quantum computation with linear optics. Nature 2001;409:46E2.
[36] Pittman TB, Jacobs BC, Franson JD. Probabilistic quantum logic operations using polarization beam splitters. Phys Rev A 2001;64:062311.
[37] Walther P, Resch KJ, Rudolph T, Schenck E, Weinfurter H, Vedral V, Aspelmeyer M, Zeilinger A. Experimental one-way quantum computing. Nature 2005;434:169–76.
[38] Kok P, Munro WJ, Nemoto K, Ralph TC, Dowling JP, Milburn GJ. Linear optical quantum computing with photonic qubits. Rev Mod Phys 2007;79:135–74.
[39] Kwiat PG, Mattle K, Weinfurter H, Zeilinger A, Sergienko AV, Shih Y. New high-intensity source of polarization-entangled photon pairs. Phys Rev Lett 1995;75:4337–41.
[40] Kwiat PG, Waks E, White AG, Appelbaum I, Eberhard PH. Ultrabright source of polarization-entangled photons. Phys Rev A 1999;60:R773.
[41] Yamada K. Silicon photonic wire waveguides: fundamentals and applications. Silicon Photon II 2011;119:1–29.
[42] Lim HC, Yoshizawa A, Tsuchida H, Kikuchi K. Stable source of high quality telecom-band polarization-entangled photon-pairs based on a single, pulse-pumped, short PPLN waveguide. Opt Express 2008;16:12460–8.

[43] Takesue H, Fukuda H, Tsuchizawa T, Watanabe T, Yamada K, Tokura Y, Itabashi S. Generation of polarization entangled photon pairs using silicon wire waveguide. Opt Express 2008;16:5721–7.
[44] Suhara T, Nakaya G, Kawashima J, Fujimura M. Quasi-phase-matched waveguide devices for generation of postselection-free polarization entangled twin photons. IEEE Photon Technol Lett 2009;21:1096–8.
[45] Martin A, Issautier A, Herrmann H, Sohler W, Ostrowsky DB, Alibart O, Tanzilli S. A polarization entangled photon-pair source based on a type-II PPLN waveguide emitting at a telecom wavelength. New J Phys 2010;12:103005.
[46] Arahira S, Namekata N, Kishimoto T, Yaegashi H, Inoue S. Generation of polarization entangled photon pairs at telecommunication wavelength using cascaded $\chi^{(2)}$ processes in a periodically poled $LiNbO_3$ ridge waveguide. Opt Express 2011;19:16032–43.
[47] Matsuda N, Le Jeannic H, Fukuda H, Tsuchizawa T, Munro WJ, Shimizu K, Yamada K, Tokura Y, Takesue H. A monolithically integrated polarization entangled photon pair source on a silicon chip. Sci Rep 2012;2:817.
[48] Fukuda H, YamadaK, Tsuchizawa T, Watanabe T, Shinojima H, Itabashi S. Polarization rotator based on silicon wire waveguides. Opt Express 2008;16:2628–35.
[49] Fukuda H, Yamada K, Tsuchizawa T, Watanabe T, Shinojima H, Itabashi S. Silicon photonic circuit with polarization diversity. Opt Express 2008;16:4872–80.
[50] Leuthold J, Koos C, Freude W. Nonlinear silicon photonics. Nat Photon 2010;4:535–44.
[51] Zhang L, Agrawal A, Kimerling LC, Michel J. Nonlinear group IV photonics based on silicon and germanium: from near-infrared to mid-infrared. Nanophotonics 2014;3:247E68.
[52] Clemmen S, Phan Huy K, Bogaerts W, Baets RG, Emplit Ph, Massar S. Continuous wave photon pair generation in silicon-on-insulator waveguides and ring resonators. Opt Exp 2009;17:16558–70.
[53] Takesue H. Entangled photon pair generation using silicon wire waveguides. EIEEE J Sel Top Quant 2012;18:1722E732.
[54] Harada K, Takesue H, Fukuda H, Tsuchizawa T, Watanabe T, Yamada K, Tokura Y, Itabashi S. Generation of high-purity entangled photon pairs using silicon wire waveguide. Opt Express 2008;16:20368–73.
[55] Fukuda H, Yamada K, Shoji T, Takahashi M, Tsuchizawa T, Watanabe T, Takahashi J, Itabashi S. Four-wave mixing in silicon wire waveguides. Opt Express 2005;13:4629–37.
[56] Foster MA, Turner AC, Sharping JE, Schmidt BS, Lipson M, Gaeta AL. Broad-band optical parametric gain on a silicon photonic chip. Nature 2006;441:960E63.
[57] James DFV, Kwiat PG, Munro WJ, White AG. Measurement of qubits. Phys Rev A 2001;64:052312.
[58] Modlawska J, Grudka A. Increasing singlet fraction with entanglement swapping. Phys Rev A 2008;78:032321.
[59] Badziag P, Horodecki M, Horocecki P, Horodecki R. Local environment can enhance fidelity of quantum teleportation. Phys Rev A 2000;62:012311.
[60] Olislager L, Safioui J, Clemmen S, Huy KP, Bogaerts W, Baets R, Emplit P, Massar S. Silicon-on-insulator integrated source of polarization-entangled photons. Opt Lett 2013;38:1960–2.
[61] Lv N, Zhang W, Guo Y, Zhou Q, Huang Y, Peng J. 1.5 μm polarization entanglement generation based on birefringence in silicon wire waveguides. Opt Lett 2013;38:2873–6.
[62] Orieux A, Eckstein A, Lematre A, Filloux P, Favero I, Leo G, Coudreau T, Keller A, Milman P, Ducci S. Direct bell states generation on a III-V semiconductor chip at room temperature. Phys Rev Lett 2013;110:160502.
[63] Horn RT, Kolenderski P, Kang D, Abolghasem P, Scarcella C, Frera AD, Tosi A, Helt LG, Zhukovsky SV, Sipe JE, Weihs G, Helmy AS, Jennewein T. Inherent polarization entanglement generated from a monolithic semiconductor chip. Sci Rep 2013:3;2314.
[64] Vallés A, Hendrych M, Svozilík J, Machulka R, Abolghasem P, Kang D, Bijlani BJ, Helmy AS, Torres JP. Generation of polarization-entangled photon pairs in a Bragg reflection waveguide. Opt Express 2013;21:10841–9.
[65] Kang D, Kim M, He H, Helmy AS. Two polarization-entangled sources from the same semiconductor chip. Phys Rev A 2015;92:013821.
[66] Kang D, Anirban A, Hemly AS. Monolithic semiconductor chips as a source for broadband wavelength-multiplexed polarization entangled photons. arXiv:1511.00903 [quant-ph].
[67] Hayat A, Ginzburg P, Orenstein M. Observation of two-photon emission from semiconductors. Nat Photon 2008;2:238–41.
[68] Boitier F, Orieux A, Autebert C, Lematre A, Galopin E, Manquest C, Sirtori C, Favero I, Leo G, Ducci S. Electrically injected photon-pair source at room temperature. Phys Rev Lett 2014;112:183901.
[69] Bonneau D, Lobino M, Jiang P, Natarajan CM, Tanner MG, Hadfield RH, Dorenbos SN, Zwiller V, Thompson MG, O'Brien JL. Fast path and polarization manipulation of telecom wavelength single photons in lithium niobate waveguide devices. Phys Rev Lett 2012;108:053601.
[70] Sansoni L, Sciarrion F, Vallone G, Mataloni P, Crespi A, Ramponi R, Osellame R. Polarization and entangled state measurement on a chip. Phys Rev Lett 2010;105:200503.
[71] Crespi A, Ramponi R, Osellame R, Sansoni L, Bongianni I, Sciarrino F, Vallone G, Mataloni P. Integrated photonic quantum gates for polarization qubits. Nat Commun 2011;2:566.
[72] Corrielli G, Crespi A, Geremia R, Ramponi R, Sansoni L, Santinelli A, Mataloni P, Sciarrino F, Osellame R. Rotated waveplates in integrated waveguide optics. Nat Commun 2014;5:4249.
[73] Migdall AL, Branning D, Castelletto S. Tailoring single-photon and multiphoton probabilities of a single-photon on-demand source. Phys Rev A 2002;66:053805.
[74] Ma X.-S, Zotter S, Kofler J, Jennewein T, Zeilinger A. Experimental generation of single photons via active multiplexing. Phys Rev A 2011;83:043814.
[75] Collins MJ, Xiong C, Rey IH, Vo TD, He J, Shahnia S, Reardon C, Krauss TF, Steel MJ, Clark AS, Eggleton BJ. Integrated spatial multiplexing of heralded single-photon sources. Nat Commun 2013;4:2582.
[76] Xiong C, Vo TD, Collins MJ, Li J, Krauss TF, Steel MJ, Clark AS, Eggleton BJ. Bidirectional multiplexing of heralded single photons from a silicon chip. Opt Lett 2013;38:5176–9.
[77] Pittman TB, Jacobs BC, Franson JD. Single photons on pseudodemand from stored parametric down-conversion. Phys Rev A 2002;66:042303.
[78] Notomi M, Yamada K, Shinya A, Takahashi J, Takahashi C, Yokohama I. Extremely large group-velocity dispersion of line-defect waveguides in photonic crystal slabs. Phys Rev Lett 2001;87:253902.
[79] Krauss TF. Slow light in photonic crystal waveguides. J Phys D Appl Phys 2007;40:2666–70.

[80] Baba T. Slow light in photonic crystals. Nature Photon 2008;2:465–73.
[81] Monat C, de Sterke M, Eggleton BJ. Slow light enhanced nonlinear optics in periodic structures. J Opt 2010;12:104003.
[82] Xiong C, Monat C, Clark AS, Grillet C, Marshall GD, Steel MJ, Li J, O'Faolain L, Krauss TF, Rarity JG, Eggleton BJ. Slow-light enhanced correlated photon pair generation in a silicon photonic crystal waveguide. Opt Lett 2011;36:3413–5.
[83] Xiong C, Collins MJ, Steel MJ, Krauss TF, Eggleton BJ, Clark AS. Photonic crystal waveguide sources of photons for quantum communication applications. IEEE J Sel Top Quant 2015; 21:1–10.
[84] Yariv A, Xu Y, Lee RK, Scherer A. Coupled-resonator optical waveguide: a proposal and analysis. Opt Express 1999;24:711–3.
[85] Davanço M, Ong JR, Shehata AB, Tosi A, Agha I, Assefa S, Xia F, Green WMJ, Mookherjea S, Srinivasan K. Appl Phys Lett 2012;100:261104.
[86] Matsuda N, Kato T, Harada K, Takesue H, Kuramochi E, Taniyama H, Notomi M. Slow light enhanced optical nonlinearity in a silicon photonic crystal coupled-resonator optical waveguide. Opt Express 2011;19:19861–74.
[87] Notomi M, Kuramochi E, Tanabe T. Large-scale arrays of ultrahigh-Q coupled nanocavities. Nat Photon 2008;2:741–7.
[88] Kuramochi E, Notomi M, Mitsugi S, Shinya A, Tanabe T, Watanabe T. Ultrahigh-Q photonic crystal nanocavities realized by the local width modulation of a line defect. Appl Phys Lett 2006;88:041112.
[89] Matsuda N, Kuramochi E, Takesue H, Notomi M. Dispersion and light transport characteristics of large-scale photonic-crystal coupled nanocavity arrays. Opt Lett 2014;39:2290–3.
[90] Matsuda N, Takesue H, Shimizu K, Tokura Y, Kuramochi E, Notomi M. Slow light enhanced correlated photon pair generation in photonic-crystal coupled-resonator optical waveguides. Opt Express 2013;21:8596–604.
[91] Takesue H, Matsuda N, Kuramochi E, Notomi M. Entangled photons from on-chip slow light. Sci Rep 2014;4:3913.
[92] Mookherjea S, Park JS, Yang S-H, Bandaru PR. Nat Photon 2008;2:90.
[93] Xia F, Sekaric L, Vlasov Y. Nat Photon 2007;1:65.
[94] Cooper ML, Gupta G, Schneider MA, Green WMJ, Assefa S, Xia F, Gifford DK, Mookherjea S. Opt Lett 2010;35:3030.
[95] Luo X, Poon AW. Opt Express 2009;17:23617.
[96] Cooper ML, Gupta G, Schneider MA, Green WMJ, Assefa S, Xia F, Vlasov YA, Mookherjea S. Statistics of light transport in 235-ring silicon coupled-resonator optical waveguides. Opt Express 2010;18:26505.
[97] Sapienza L, Thyrrestrup H, Stobbe S, Garcia PD, Smolka S, Lodahl P. Cavity quantum electrodynamics with anderson-localized modes. Science 2010;327:1352–5.
[98] Lian J, Sokolov S, Yüce E, Combrié S, De Rossi A, Mosk AP. Dispersion of coupled mode-gap cavities. Opt Lett 2015;40:4488–91.
[99] Caselli N, Riboli F, La China F, Gerardino A, Li L, Linfield EH, Pagliano F, Fiore A, Intonti F, Gurioli M. Tailoring the photon hopping by nearest and next-nearest-neighbour interaction in photonic arrays. ACS Photonics 2015;2:565–71.
[100] Zou XY, Wang LJ, Mandel L. Violation of classical probability in parametric down-conversion. Opt Commun 1991;84:351–4.
[101] Franson JD. Bell inequality for position and time. Phys Rev Lett 1989;62:2205E208.
[102] Kuzmich A, Bowen WP, Boozer AD, Boca A, Chou CW, Duan L-M, Kimble HJ. Generation of nonclassical photon pairs for scalable quantum communication with atomic ensembles. Nature 2003;423:731–4.
[103] Meany T, Ngah LA, Collins MJ, Clark AS, Williams RJ, Eggleton BJ, Steel MJ, Withford MJ, Alibart O, Tanzilli S. Hybrid photonic circuit for multiplexed heralded single photons. Laser Photonics Rev 2014;8:L42–6.
[104] Silverstone JW, Bonneau D, Ohira K, Suzuki N, Yoshida H, Iizuka N, Ezaki M, Natarajan CM, Tanner MG, Hadfield RH, Zwiller V, Marshall GD, Rarity JG, O'Brien JL, Thompson MG. On-chip quantum interference between silicon photon-pair sources. Naure Photon 2014;8:104–8.
[105] Jöns KD, Rengstl U, Oster M, Hargart F, Heldmaier M, Bounouar S, Ulrich SM, Jetter M, Michler P. Monolithic on-chip integration of semiconductor waveguides, beamsplitters and single-photon sources. arXiv:1403.7174 [quant-ph].
[106] Prtljaga N, Coles RJ, O'Hara J, Royall B, Clarke E, Fox AM, Skolnick MS. Monolithic integration of a quantum emitter with a compact on-chip beam-splitter. Appl Phys Lett 2014;104:231107.
[107] Harris NC, Grassani D, Simbula A, Pant M, Galli M, Baehr-Jones T, Hochberg M, Englund D, Bajoni D, Galland C. Integrated source of spectrally filtered correlated photons for large-scale quantum photonic systems. Phys Rev X 2014;4:041047.
[108] Silverstone JW, Santagati R, Bonneau D, Strain MJ, Sorel M, O'Brien JL, Thompson MG. Qubit entanglement between ring-resonator photon-pair sources on a silicon chip. Nat Commun 2015;6:7948.
[109] Murray E, Ellis DJP, Meany T, Floether FF, Lee JP, Griffiths JP, Jones GAC, Farrer I, Ritchie DA, Bennett AJ, Shields AJ. Quantum photonics hybrid integration platform. Appl Phys Lett 2015;107:171108.
[110] Bonneau D, Engin E, Ohira K, Suzuki N, Yoshida H, Iizuka N, Ezaki M, Natarajan CM, Tanner MG, Hadfield RH, Dorenbos SN, Zwiller V, O'Brien JL, Thompson MG. Quantum interference and manipulation of entanglement in silicon wire waveguide quantum circuits. New J Phys 2012;14:045003.
[111] Wang J, Santamato A, Jiang P, Bonneau D, Engin E, Silverstone JW, Lermer M, Beetz J, Kamp M, Höfling S, Tanner MG, Natarajan CM, Hadfield RH, Dorenbos SN, Zwiller V, O'Brien JL, Thompson MG. Gallium arsenide (GaAs) quantum photonic waveguide circuits. Opt Commun 2014;327:49–55.
[112] Smith BJ, Kundys D, Thomas-Peter N, Smith PGR, Walmsley IA. Phase-controlled integrated photonic quantum circuits. Opt Express 2009;17:13516–25.
[113] Sohma S, Watanabe T, Ooba N, Itoh M, Shibata T, Takahashi H. Silica-based PLC type 32E2 optical matrix switch. ECOC 2006;1–2.
[114] Hibino Y. Recent advances in high-density and large-scale AWG multi/demultiplexers with higher index-contrast silica-based PLCs. IEEE J Sel Top Quant 2002;8:1090–101.
[115] Matsuda N, Shimizu R, Mitsumori Y, Kosaka H, Edamatsu K. Observation of optical-fibre Kerr nonlinearity at the single-photon level. Naure Photon 2009;3:95–8.

[116] Matsuda N, Karkus P, Nishi H, Tsuchizawa T, Munro WJ, Takesue H, Yamada K. On-chip generation and demultiplexing of quantum correlated photons using a silicon-silica monolithic photonic integration platform. Opt. Express 2014;22:22831–40.
[117] Nishi H, Tsuchizawa T, Watanabe T, Shinojima H, Park S, Kou R, Yamada K, Itabashi S. Monolithic integration of a silica-based arrayed waveguide grating filter and silicon variable optical attenuators based on p-i-n carrier-injection structure. Appl Phys Express 2010;3:102203.
[118] Tsuchizawa T, Yamada K, Watanabe T, Sungbong P, Nishi H, Kou R, Shinojima H, Itabashi S. Monolithic integration of silicon-, germanium-, and silica-based optical devices for telecommunications applications. IEEE J Sel Top Quant 2011;17:516–25.
[119] Hiraki T, Nishi H, Tsuchizawa T, Kou R, Fukuda H, Takeda K, Ishikawa Y, Wada K, Yamada K. Si-Ge-silica monolithic integration platform and its application to a 22-Gb/s 16-ch WDM receiver. Photonics J IEEE 2013;5:4500407.
[120] Yoshino K, Fujiwara M, Tanaka A, Takahashi S, Nambu Y, Tomita A, Miki S, Yamashita T, Wang Z, Sasaki M, Tajima A. High-speed wavelength-division multiplexing quantum key distribution system. Opt Lett 2012;37:223–5.
[121] Schaeff C, Polster R, Lapkiewicz R, Fickler R, Ramelow S, Zeilinger A. Scalable fiber integrated source for higher-dimensional path-entangled photonic quNits. Opt Express 2012;20:16145–53.
[122] Schaeff C, Polster R, Huber M, S. Ramelow and Zeilinger A. Experimental access to higher-dimensional entangled quantum systems using integrated optics. Optica 2015;2:523–9.
[123] Yamazaki H, Yamada T, Goh T, Sakamaki Y, Kaneko A. 64 QAM modulator with a hybrid configuration of silica PLCs and $LiNbO_3$ phase modulators. IEEE Photon Technol Lett 2010;22:344–6.
[124] Takesue H. Entangling time-bin qubits with a switch. Phys Rev A 2014;89:062328.